Pharm Res (2013) 30:1161–1175
DOI 10.1007/s11095-012-0952-9

RESEARCH PAPER

Cellular Uptake Mechanisms of Novel Anionic siRNA Lipoplexes

Mamta Kapoor • Diane J. Burgess

Received: 2 November 2012 / Accepted: 30 November 2012 / Published online: 13 December 2012

ABSTRACT

Purpose To investigate cellular uptake pathways of novel anionic siRNA-lipoplexes as a function of formulation composition.

Methods Anionic formulations with anionic lipid/Ca^{2+}/siRNA ratio of 1.3/2.5/1 (AF1) and 1.3/0.3/1 (AF2) were utilized. Uptake mechanisms were investigated using uptake inhibition and co-localization approaches in breast cancer cells. Actin-mediated uptake was investigated using actin polymerization and rearrangement assays. Silencing efficiency and endosomal escaping capability of lipoplexes were evaluated. The cationic formulation Lipofectamine-2000 was used as a control.

Results Anionic lipoplexes entered the breast cancer cells *via* endocytosis specifically *via* macropinocytosis or *via* both macropinocytosis and HSPG (heparin sulfate proteoglycans) pathways, depending on the Ca^{2+}/siRNA ratio. Additionally, uptake of these lipoplexes was both microtubule and actin dependent. The control cationic lipid-siRNA complexes (Lipofectamine-2000) were internalized *via* both endocytic (phagocytosis, HSPG) and non-endocytic (membrane fusion) pathways. Their uptake was microtubule independent but actin dependent. Silencing efficiency of the AF2 formulation was negligible mainly due to poor endosomal release (rate-limiting step).

Conclusions Formulation composition significantly influences the internalization mechanism of anionic lipoplexes. Uptake mechanism together with formulation bioactivity helped in identification of the rate-limiting steps to efficient siRNA delivery. Such studies are extremely useful for formulation optimization to achieve enhanced intracellular delivery of nucleic acids.

Electronic supplementary material The online version of this article (doi:10.1007/s11095-012-0952-9) contains supplementary material, which is available to authorized users.

M. Kapoor • D. J. Burgess (✉)
Department of Pharmaceutical Sciences, School of Pharmacy
University of Connecticut, 69 N Eagleville Rd, Unit 3092
Storrs, Connecticut 06269, USA
e-mail: d.burgess@uconn.edu

KEY WORDS anionic lipoplexes · endocytosis · formulation composition · siRNA · uptake mechanism/pathway

INTRODUCTION

Owing to the specificity and high potency of small interfering RNA (siRNA), the potential of siRNA therapeutics is being explored for the treatment of many diseases such as cancer and HIV(1,2). However, the delivery of siRNA therapeutics is challenging due to their susceptibility to nuclease degradation, their low cellular uptake and poor endosomal escape (3). To combat these issues, several non-viral vectors such as cationic liposomes have been employed (4,5). Cationic lipid formulations facilitate efficient siRNA delivery but may cause severe cytotoxicity and/or serum inactivation probably due to their cationic charge (6). Accordingly, formulations based on anionic lipids are desirable (7,8). Recently, anionic lipid based siRNA lipoplexes (anionic liposomes, calcium, siRNA) were developed that were shown to be safe and effective in breast cancer cells (4,9,10).

Cellular uptake of nanoparticle-based delivery systems, commonly occurs by endocytosis (11). Endocytosis can be further classified into phagocytosis (in tumor cells and specialized cells such as macrophages), clathrin-mediated, caveolae-mediated, clathrin-caveolae independent endocytosis (*e.g.* proteoglycans) and macropinocytosis. Some formulations especially those that are liposome-based have been reported to enter *via* non-endocytic pathways *e.g.* fusion (12). These are energy-independent pathways that can occur even at low temperatures (13,14).

The uptake pathway/mechanism of siRNA formulations mainly depends on the type of delivery carrier and the formulation composition as these factors may influence particle-cell interactions. Additionally, the efficiency of siRNA delivery particularly depends on the uptake pathway as each pathway involves a series of events that exposes the

siRNA delivery system to different chemical environments (*e.g.* pH, ions *etc.*) (11). Therefore, knowledge of the uptake pathway/mechanism for a specific delivery system is mandatory to develop efficient formulations for enhanced biomolecular delivery. Also the effect of formulation composition on uptake mechanisms must be carefully examined. There are two main approaches to elucidate cellular uptake mechanisms: (a) use of pharmacological inhibitors that interfere with a specific endocytosis mechanism resulting in exclusion, and (b) co-localization of specific endocytosis markers, with the nanoparticle formulations (15). Simultaneous application of both the approaches, ensures accurate determination of the uptake mechanism.

Knowledge of the uptake mechanism is helpful in recognizing the biological barrier(s) to efficient intracellular delivery and can be utilized to explain formulation efficiency. This facilitates optimization of formulations to achieve improved delivery. In the present work, the uptake mechanism of novel anionic siRNA lipoplexes (anionic liposomes, Ca^{2+} and siRNA) constituting the new siRNA carrier (DOPG/DOPE anionic liposomes, Ca^{2+}) was elucidated as a function of formulation composition (lipid/Ca^{2+}/siRNA ratios), in unfixed breast cancer cells. Uptake inhibition of the lipoplex formulations was evaluated using FACS (fluorescence-assisted cell sorting) and fluorescence microscopy. Confocal microscopy was utilized to determine the co-localization of lipoplex formulations with endocytic markers. Additionally, actin rearrangement and actin polymerization assays were performed to investigate the role of actin in the uptake process. GFP knockdown studies and confocal microscopy were performed to evaluate the silencing efficiency and endosomal escaping capability of lipoplex formulations, respectively.

MATERIALS AND METHODS

Materials

The lipids DOPG (1,2-dioleoyl-*sn*-glycero-3-phospho-(1′-rac-glycerol), DOPE (1,2-dioleoyl-*sn*-glycero-3- phosphoethanolamine), C-DOPE (1,2-dioleoyl-*sn*-glycero-3-phosphoethanolamine-N-(carboxyfluorescein) (ammonium salt)) were purchased from Avanti polar lipids Inc (Alabama, USA). Fluorescent-siRNA (alexa-488 siRNA) was gifted by Alnylam Pharmaceuticals (Cambridge, MA). Alexa-488 siRNA sequence: antisense 5′-CUUACGCUGAGUACUUC GAdTdT-3′, sense 5′-alexa488-UCGAAGUACUCAG CGUAAGdTdT-3′ (dT:desoxy-thymidine). Silencer® eGFP siRNA (or anti-eGFP siRNA, eGFP- enhanced green fluorescent protein) was purchased from Ambion. Anti-eGFP siRNA sequence: antisense 5′-GAACUUCAGGGUCAGCUUG cc-3′, sense 5′-CAAGCUGACCCUGAAGUUCtt-3′ (base in lower case: 3′ overhang). (5-N,N dimethyl amiloride (DMA), filipin complex, chlorpromazine hydrochloride, cytochalasin D, nocodazole, wortmannin, sodium chlorate and calcium chloride were purchased from Sigma. For cell culture, MDA-MB-231 or breast cancer cells (no eGFP from ATCC, stably transfected with eGFP from Cell Biolabs Inc., CA) and penicillin-streptomycin antibiotic solution (ATCC) were used. Dulbecco' Modified Eagle's medium (DMEM), Modified Eagle's medium - non essential amino acids (MEM-NEAA), Hank's balanced salt solution (HBSS), Opti-MEM I, L-glutamine, heat inactivated fetal bovine serum (FBS), alexa fluor® 647-phalloidin, rhodamine-B dextran (70 kDa, neutral), alexa fluor® 555-cholera toxin B subunit (CTB), Hoechst 33342, trypan blue solution (0.4%) and Lipofectamine™2000 were purchased from Invitrogen.

Alexa 488-siRNA and MDA-MB-231 cells (no eGFP) were utilized for the following studies except the silencing efficiency studies. For the latter anti-eGFP siRNA and MDA-MB-231 cells stable transfected with eGFP were utilized. Sequence specificity of anti eGFP-siRNA was established by comparing its silencing efficiency (dose dependent knockdown) with the scrambled or negative control siRNA (no silencing at any dose investigated).

Lipoplex Preparation and Characterization

Anionic lipoplex formulations (AF) were prepared as described previously (10). Briefly, anionic liposomes (100 nm) were prepared with the anionic lipid DOPG and the zwitterion lipid DOPE (DOPG/DOPE 40:60 molar ratio) in 10 mM HEPES buffer, pH 7.4, using the film hydration method followed by extrusion. These liposomes were complexed with siRNA (200 μM stock) *via* calcium ions (4.3 M, $CaCl_2$ stock). Calcium was mixed with siRNA (5 min) in appropriate amount followed by addition of anionic liposomes (10 min) to obtain anionic lipoplexes with desired anionic lipid/Ca^{2+}/siRNA molar charge ratio. The lipoplexes were incubated for 15 min at room temperature. To assess the effect of formulation composition on the uptake mechanism, two anionic lipoplex formulations with different lipid/Ca^{2+}/siRNA molar charge ratios were prepared – AF1 with 1.3/2.5/1 ratio, AF2 with 1.3/0.3/1 ratio. AF1 was selected as it had previously been shown to be the most efficient with negligible toxicity compared to other anionic formulations, Ca^{2+}-siRNA control and Lipofectamine 2000 lipoplexes (9,10). AF2 was selected to understand the role of the Ca^{2+}/siRNA ratio on the uptake mechanism.

To examine the effect of the type of delivery carrier, the uptake mechanism of lipoplexes formed with Lipofectamine2000 (CF) was investigated. Cationic lipoplex formulation (CF) was prepared with Lipofectamine 2000 (LF2000) and siRNA, using the same lipid and siRNA concentrations

as in the case of anionic lipoplexes (1 μg/mL LF2000 for 10 nM siRNA).

Ca^{2+}-siRNA control was prepared using the same method as the anionic lipoplexes except for the addition of anionic liposomes. For preparation of fluorescently labeled anionic liposome control, liposomes were prepared with a molar composition of 40:59:1 (DOPG/DOPE/C-DOPE), using the above mentioned procedure.

Lipoplex formulations (AF1, AF2 and CF) were characterized for particle size and zeta potential using a Malvern Zetasizer ZS90. For this purpose, lipoplexes were prepared in 10 mM HEPES, pH 7.4 and the measurements were performed at 25°C in triplicate. For particle size, the intensity distribution was considered. For zeta potential, the net surface charge was measured using a universal 'dip' cell containing 1 mL of sample. siRNA loading efficiency of the lipoplexes was evaluated using previously published method (10). For this study the samples were prepared in cell culture media to mimic the actual siRNA loading in cell culture conditions.

Cell Culture

Breast cancer cells (MDA-MB-231) (with or without eGFP) were cultured in DMEM with 10% FBS, 2 mML-glutamine, 0.1 mM MEM-NEAA, and 1% antibiotics (penicillin-streptomycin). The cells were maintained at 37°C in 5% CO_2 atmosphere. The media was changed once in every 2–3 days.

Uptake Inhibitors

To evaluate the uptake mechanism, low temperature conditions (4°C) or specific pharmacological inhibitors were employed to block one or more uptake pathways. For pharmacological inhibitors, a broad concentration range for each inhibitor was selected (Table I) and evaluated for cytotoxicity (propidium iodide assay) as well as cellular uptake of the formulations (fluorescence-activated cell sorting or FACS). From the concentration range investigated for each drug, the concentration beyond which there was no effect on the cellular uptake of the formulations (AF1, AF2, CF) and the drug cytotoxicity was low, was selected. For example, increase in the concentration of the filipin complex (caveolae-inhibitor) from 1 μg/mL to 5 μg/mL showed no effect on the uptake of AF1, AF2 or CF. However, an increase in cytotoxicity from 3 to 15% occurred when the drug concentration was increased from 1 to 5 μg/mL (data not shown). Therefore a filipin concentration of 1 μg/mL was selected. Other drug concentrations were optimized similarly. The final concentration of the pharmacological inhibitors is listed in Table I.

For inhibition studies, the cells were pre-incubated with pharmacological inhibitors for 30 min (sodium chlorate for 24 h) at 37°C followed by transfection with lipoplex formulations (AF1, AF2, CF) for 4 h. For formulation uptake at low temperature (energy-independent) the cells were maintained at 4°C for 30 min and then incubated with the lipoplex formulations at the same temperature for 4 h. The lipoplexes were incubated in the presence of the inhibitors or at 4°C. However, sodium chlorate was removed prior to transfection with the lipoplexes (16). After 4 h incubation, the cells were washed with HBSS and incubated with trypan blue (0.008%) for 10 min to quench the extracellular fluorescence (17). Subsequently, the cells were assayed using FACS or fluorescence microscopy. Lipoplex uptake in the absence of inhibitors and cellular uptake of untreated cells (without lipoplexes) was also determined. All transfections were performed in the presence of serum. The efficiency of trypan blue quenching was established using a control experiment (Supplementary Material Fig. S1).

FACS Analysis

Cellular uptake of lipoplex formulations (40 nM alexa-488 siRNA) was quantified using FACS. 1.25×10^5 cells/well were seeded in 24 well plates in 500 μL cell culture media, and allowed to grow at 37°C. After 24 h, the cells were transfected with 200 μL of lipoplex formulations (AF1, AF2, CF) in Opti-MEM I for 4 h, in the presence or absence of inhibitors (incubation time as described above). The cells were treated with trypan blue, trypsinized, resuspended in culture media and analyzed using the FACS instrument (BD FACS Calibur, San Jose, CA with Cell Quest software) with 488 nm laser excitation. 10,000 cells were collected for each sample and the data was analyzed using Flow Jo software (version 9.0). Gating was performed on forward scatter-side scatter plots (FSC-SSC) to eliminate the dead cells and cell debris. Untreated cells, siRNA alone, lipid + siRNA mixtures, Ca^{2+}-siRNA complexes (Ca^{2+} to siRNA ratio of 2.5/1) and fluorescent-labeled anionic liposomes were used as controls. The results were reported as fold-uptake that was obtained by dividing the median fluorescence intensity (in RFU) of samples (formulations) by the median fluorescence intensity of untreated cells (normalized data). For inhibition studies, cellular uptake (fluorescence intensity) of lipoplexes in the presence of inhibitors was normalized by their uptake in the absence of inhibitors (control sample, 100% uptake). Represented data is an average of three independent experiments in duplicate.

Fluorescence Microscopy

Cellular uptake of lipoplexes in the presence or absence of inhibitors was visualized using fluorescence microscope. 6×

Table I Uptake Inhibitors, their Functions and Concentrations

Treatment	Inhibits Pathway	Mechanism	Concentration Range	Final Concentration
4°C	Endocytosis	Energy depletion	-	-
Chlorpromazine hydrochloride	Clathrin-mediated endocytosis	Dissociation of clathrin lattice	10–50 μM	10 μM
Filipin complex	Caveole	Cholesterol binding	0.5–20 μg/mL	1 μg/mL
5-N,N dimethyl amiloride (DMA)	Macropinocytosis	Inhibits the Na^+/H^+ exchange protein	10–500 μM	250 μM
Nocodazole	Microtubular transport	Microtubule depolymerization	5–100 μM	10 μM
Cytochalasin D	Actin based transport	Actin depolymerization	0.5–40 μM	1 μM
Wortmannin	Macropinocytosis, phagocytosis	Phosphoinositide 3-kinase (PI3K) inhibitor	10–200 nM	100 nM
Sodium Chlorate	Heparin sulfate proteoglycans (HSPG)	Inhibits sulfyrase enzyme required for biosynthesis of HSPG	50–200 mM	100 mM

10^4 cells/well were seeded in 8-well chamber slides (Lab-Tek II, Thermo Scientific) and incubated for 24 h at 37°C. The cells were transfected with alexa-488 siRNA lipoplexes (prepared with 14 nM (AF1, CF) or 56 nM siRNA (AF2)) for 4 h, with or without inhibitors. Further, the cells were washed, quenched and imaged using Nikon TiE fluorescence microscope with Andor EMCCD iXon897 camera. For each sample, five fields were viewed with a 10X objective with 80–100 cells/view. The images were analyzed using Image J software (NIH). Image capturing and analysis was performed for controls (lipoplexes without inhibitors) and for treated samples (lipoplexes with inhibitors) under the same conditions to allow a rational comparison. Untreated cells and siRNA alone were used as controls.

Formulation Internalization and Co-localization Studies Using Confocal Microscopy

Spinning disc confocal microscope (Andor Technology, Tokyo, Japan with iQ2 live cell imaging software) was utilized to visualize the cellular internalization and subcellular localization of fluorescent-siRNA delivered using the lipoplex formulations. For this purpose, breast cancer cells were plated in 8-well chamber slides at a density of 9×10^4 cells/well and allowed to attach overnight. On the following day, the cells were transfected with lipoplexes (prepared with 40 nM siRNA) for 2 h at 37°C and endocytosis markers (70 kDa rhodamine-B-dextran for macropinosomes or alexa555-CTB for caveolae) were added during the last 30 min. The cells were washed with HBSS, quenched with trypan blue, incubated with nuclear stain Hoechst 33342 (1 μg/mL in Opti-MEM media) and immediately viewed without fixation using the confocal microscope. The images were obtained with a 40X oil objective using 405 nm, 488 nm and 561 nm excitation lasers for Hoechst 33342, alexa-488 and rhodamine-B/alexa-555, respectively. During imaging, the cells were maintained at 37°C, 5% CO_2 and 75% relative humidity atmosphere. Five fields of view were selected for each sample with 2–6 cells/view and z-sectioning was performed in each of these fields. The extent of co-localization was quantified using the Image J software with JACoP plugin (18). Both Mander's correlation coefficient (MCC) and Pearson's correlation coefficient (PCC) were obtained for the entire z-stack/view/sample and the represented values for each sample are an average from five fields of view. Laser settings were chosen to avoid signal bleed-through and maintain a high signal to noise ratio. The laser settings were kept constant during image acquisition to allow quantitative comparison of the fluorescence intensities.

Determination of Punctate to Diffused Staining Ratio (Endosomal Escaping Capability) Using Confocal Microscopy

MDA-MB-231 cells were plated (0.1×10^6 cells/well) in 8-well chamber slides. The following day, the cells were transfected with lipoplex formulations (prepared with alexa-488 siRNA) for 4 h, washed, typan blue quenched and imaged using confocal microscope with a 40X oil objective (live cell imaging). Five fields of view were selected for each sample and Z-sectioning was performed for each of these fields (n=5). Using a previously published method without modification[10], average punctate to diffused staining ratio (P/D ratio) was obtained for each sample. Untreated cells, siRNA alone, Ca^{2+}-siRNA mixture and lipid + siRNA mixture were used as negative controls.

Actin Polymerization Assay

This assay was performed to evaluate the effect of lipoplexes on actin polymerization in the presence of actin depolymerizer

(cytochalasin D). For this purpose, the cells were plated in 8-well chamber slides (9×10^4 cells/well, grown overnight) and incubated with cytochalasin D (1 μM) for 30 min. This was followed by transfection with lipoplexes (AF1, AF2 or CF with 40 nM siRNA) for 4 h. The cells were HBSS washed, quenched and fixed using 3.5% paraformaldehyde for 20 min. Thereafter the cells were permeabilized with 0.3% Triton-X100 with 0.1% BSA (5 min), and blocked with 5% BSA (30 min). Subsequently, actin filaments were labeled using alexa 647-phalloidin (30 min). The cells were washed three times with PBST (0.05% Tween 20 in 1X PBS) and viewed using the spinning disc confocal microscope with a 60X oil objective and 640 nm laser excitation. The same camera settings were used to capture images of all the samples. Image analysis was performed using the Image J software. Untreated cells and cells transfected with lipoplexes in the absence of cytochalasin D, were used as negative controls. Other controls were Ca^{2+}-siRNA complexes (Ca^{2+} to siRNA ratio of 2.5/1), calcium alone and anionic liposomes.

Membrane Ruffling and Actin Reorganization

To evaluate the role of actin on the uptake of various lipoplex formulations, ruffling of the plasma membrane and rearrangement of the cytoskeletal actin was examined. For this purpose, a previously described method was used with slight modifications (19). Briefly, before incubation with lipoplex formulations, the cells (9×10^4 cells/well, grown overnight) were kept in serum-free media for 2 h to inhibit serum induced cell ruffling. This was followed by 30 min incubation with lipoplexes (AF1, AF2 or CF with 40 nM siRNA). The cells were washed with HBSS, quenched, fixed, permeabilized and stained for actin using the above mentioned procedure (actin polymerization assay). The images were obtained using confocal microscope with a 60X oil objective. The same camera settings were used to capture images of all samples and image analysis was performed using Image J software. Untreated cells were used as a negative control.

Propidium Iodide Assay

The cytotoxicity of the drugs (pharmacological inhibitors) at optimal concentrations, and of the lipoplex formulations (AF1, AF2, CF), was evaluated using propidium iodide (PI) that permeates into the dead and dying cells. For this purpose, 1.25×10^5 cells/well were seeded in 24 well plates and allowed to grow for a day at 37°C. To evaluate the cytotoxicity of inhibitors, the cells were incubated with inhibitors (concentrations as shown in Table I) for 30 min followed by addition of 200 μL Opti-MEM I media. The cells were incubated for another 4 h, washed with HBSS, trypsinized, reconstituted in fresh culture media and analyzed using FACS. For sodium chlorate, the incubation time with the cells was 24 h and the drug was removed 4 h before sample analysis. The lipoplexes were incubated with breast cancer cells for 4 h to evaluate their cytotoxicity. PI (final concentration 5 μg/mL) was added to the samples and incubated for 1–2 min prior to sample analysis *via* FACS. The results were reported as percentage PI positive cells normalized to untreated cells. Presented data is an average of two independent experiments each time in duplicate.

Silencing Efficiency

Silencing efficiency of lipoplex formulations was evaluated using a previously published method (9). Briefly, MDA-MB-231 cells stably transfected with eGFP (Cell Biolabs Inc., CA) (only used for this study), were plated (5×10^3 cells/well) in black 96 well plates and grown overnight (in DMEM with 10% serum). On the day of the experiment, the cells were treated with lipoplex formulations (prepared with anti-eGFP siRNA- only used for this study) and incubated at 37°C in 5% CO_2 atmosphere. After 48 h, the cells were washed with buffer and the GFP expression of the cells was determined using fluorescence spectrophotometer (Spectramax Gemini XPS, Molecular Probes, with λ_{ex}=488 nm, λ_{em}=525 nm). The resulting fluorescence activity (RFU) was normalized for the amount of protein (μg) using the BCA assay (Pierce) to obtain normalized GFP expression. Percentage silencing efficiency was obtained using the following formula:

$$\%\,\text{Silencing efficiency} = 100 - \left(\frac{\text{GFP expression from sample} * 100}{\text{GFP expression from untreated cells}}\right)$$

Untreated cells, anti-eGFP siRNA alone, scrambled siRNA (negative control siRNA provided with the anti-eGFP siRNA obtained from Ambion) and lipid + siRNA mixture were used as negative controls (n=6).

Statistics

For comparison of two samples at a time, Student t-test was utilized. For comparison of several groups to a control group, one-way ANOVA with Dunnett's post-test was used.

RESULTS

Characterization and Cytotoxicity Studies

Lipoplex formulations (AF1, AF2, CF) prepared using the above mentioned method, were characterized for particle size, surface charge and siRNA loading. As shown in Table II, the particle size of AF1 was approximately three times that of AF2 whereas the size of CF was twice that of

Table II Physicochemical Properties of Anionic and Cationic Lipoplex Formulations

Formulation	Anionic lipid/Ca2+/siRNA ratio	Particle size (nm)	Zeta potential (mV)	Loading efficiency (%)
AF1	1.3/2.5/1	324.2 ± 19.6	(−22.9) ± 0.6	30.0 ± 2.0
AF2	1.3/0.3/1	114.2 ± 13.9	(−8.8) ± 2.2	100.0 ± 1.5
CF	-	217.9 ± 18.8	(±15.7) ± 2.1	100.0 ± 3.0

[a] Loading efficiencies were evaluated using previously published method (10)

AF2. For schematic representation of the formed anionic lipoplexes, see reference 10.

As expected, the zeta potential values of the anionic lipoplexes were negative and the charge of AF1 was almost twice that of AF2. The surface charge of CF was positive and was lower than that of the cationic liposomes (+53 mV). siRNA loading efficiency of AF1 and CF was almost 100% whereas it was around 30% in case of AF2 formulation (Table II). The propidium iodide assay revealed that the cytotoxicity of all formulations was less than 5% (Fig. 1). The high cell viability of the lipoplexes was further confirmed with actin staining that showed intact cell membrane and cytoskeleton (Fig. 5). Selected concentrations of the pharmacological inhibitors also showed cytotoxicity of less than 10% (Fig. 1).

Internalization of Anionic Lipoplexes

To assess whether the labeled siRNA (in lipoplexes) was internalized rather than being on the cell surface, confocal z-sectioning of the cells incubated with lipoplexes for 2 h was performed. The cells showed green punctuates (alexa-488 siRNA) in the perinuclear region predominantly in the central z-sections, indicating that the particles are inside the cells and not on the cell surfaces (Fig. 2a). Internalization of these particles was observed to increase with time (data not shown). The cationic formulation (CF) was shown to be internalized as occurs in the case of the anionic formulations (Fig. 2a).

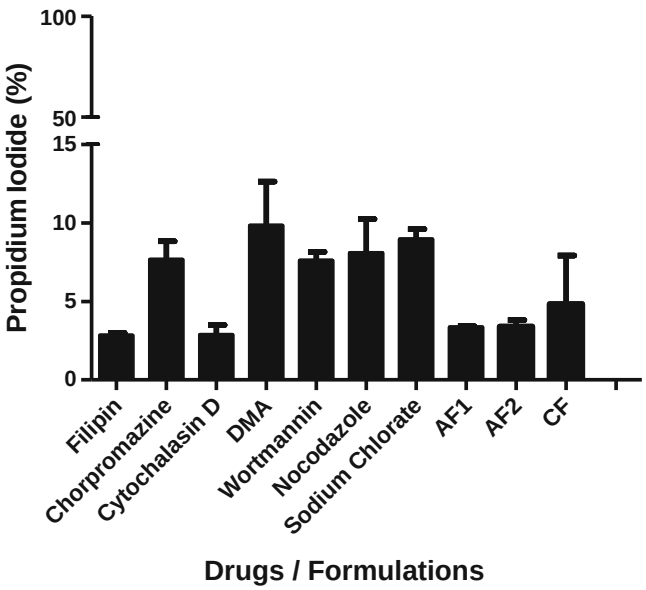

Fig. 1 Percentage propidium iodide stained cells representing the cytotoxicity of the pharmacological inhibitors (30 min incubation except sodium chlorate), and the lipoplex formulations (AF1, AF2, CF) (4 h incubation). The results are an average of two independent experiments in duplicate. Mean ± SD.

Uptake Mechanisms

For accurate determination of the internalization mechanism, it is imperative to account for only the internalized particles and not those attached onto the cell surface. Therefore a protocol based on trypan blue, known to quench the extracellular fluorescence (17) was optimized and employed before each analysis (Supplementary Material Fig. S1). Using this optimized sample preparation method, cellular uptake of the lipoplexes was evaluated quantitatively using FACS and qualitatively using fluorescence microscopy. As shown in Fig. 3a, the uptake of AF1 (13-fold) in the absence of inhibitors, was almost twice that of AF2 (7-fold). Lower uptake of AF2 was also evident in the FACS histograms (Fig. 3b). This justifies the need for higher siRNA dose of AF2 (56 nM siRNA) compared to AF1 (14 nM siRNA) for improved signal in fluorescence microscopy studies. Uptake of CF was observed to be significantly lower than AF1 (Fig. 3a, b).

To evaluate cellular uptake at low temperature, the lipoplex formulations were incubated at 4°C (at 37°C for control). As shown in Fig. 3c, uptake of the anionic lipoplexes was almost completely inhibited (98–99% inhibition) at 4°C when compared to their uptake at 37°C. Uptake of the cationic lipoplexes (CF) was 83% inhibited at 4°C compared to 37°C, indicating that a considerable amount (17%) was internalized even at low temperatures (Supplementary Material Fig. S2 for histograms).

To evaluate the involvement of clathrin and caveole-mediated uptake pathways in the internalization of the anionic formulations, breast cancer cells were treated with chlorpromazine HCl or filipin (inhibitors of the well characterized clathrin or caveolae-mediated uptake pathways, respectively) (17,20). As shown in Fig. 3d, e, there was no significant uptake inhibition of either of the anionic lipoplexes (AF1 or AF2) in

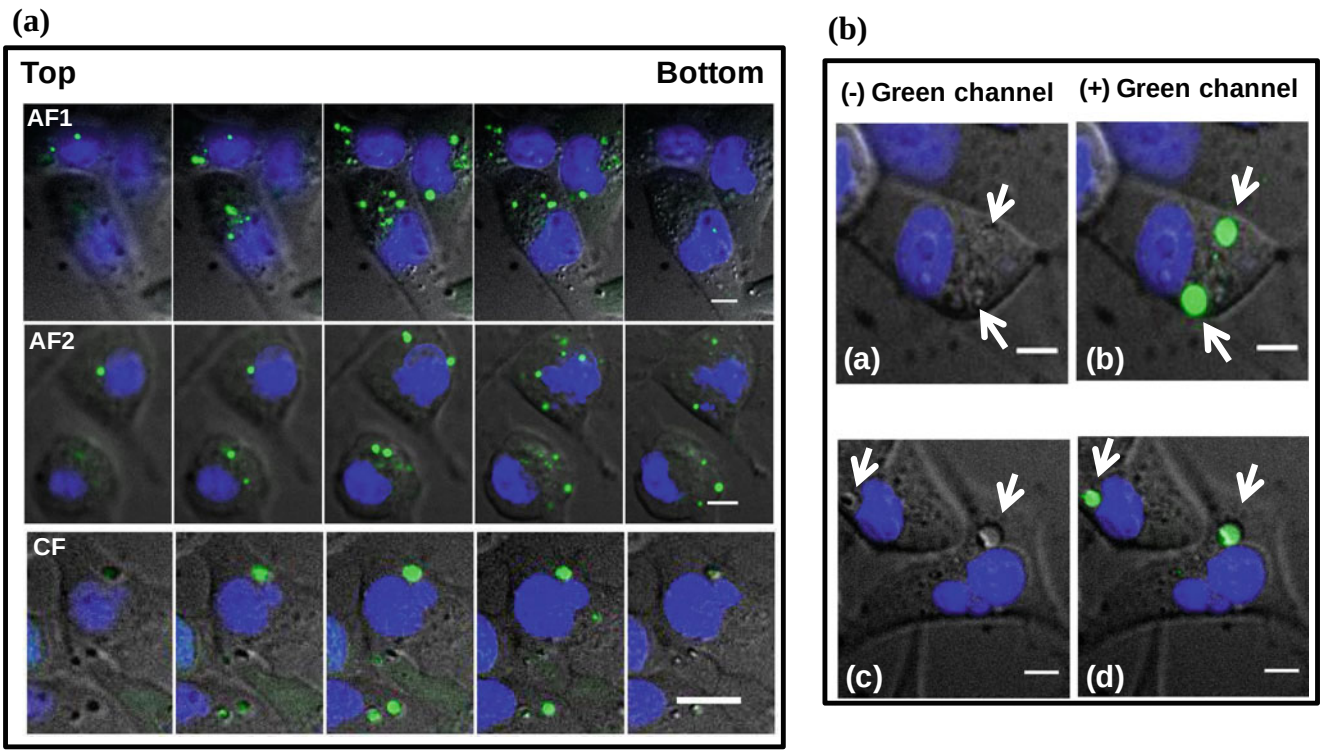

Fig. 2 (**a**) Confocal z-sections (Δz: 2 μm) representing internalization of lipoplex formulations prepared with alexa-488 siRNA (green), after 4 h incubation in breast cancer cells. (**b**) Endocytic vesicles (white arrows) formed with AF2 (a,b) or CF (c,d). The morphology of the vesicles formed with AF2 (macropinosomes) was distinctive from that of the CF vesicles (phagocytic cups). Blue represents the nucleus stained with Hoechst 33342. Scale bar 10 μm.

the presence of these drugs. Similarly, internalization of CF was unaffected by either of the two drugs (Fig. 3f). These results indicated that uptake of the three lipoplexes was clathrin and caveolae independent.

The cells were treated with DMA to assess the role of another well-characterized endocytic mechanism (macropinocytosis) on the uptake of the anionic formulations (21). Microscopic visualization showed significant uptake inhibition of AF1 and AF2 with DMA (Fig. 4). FACS analysis showed this uptake inhibition to be 54% and 98% for AF1 and AF2, respectively (Fig. 3d, e). On the other hand, the uptake of the cationic lipoplexes (CF) was not significantly affected by DMA (Fig. 3f and 4) (Supplementary Material Fig. S3 for histograms). Uptake of Ca^{2+}-siRNA and the anionic liposome control was also reduced on the addition of DMA by 52% and 87%, respectively (Supplementary Material Fig. S4). To reevaluate the role of macropinocytosis in the uptake of the anionic lipoplexes, another drug (wortmannin that inhibits PI3K transport protein essential for macropinocytosis) was employed (22). As shown in the Fig. 3d, e and 4, wortmannin reduced the uptake of the anionic lipoplexes which was quantified to be 61% and 58% for AF1 and AF2, respectively. There was also significant inhibition (16%) of CF uptake (Fig. 3f).

To further substantiate the role of macropinocytosis on the uptake of the anionic lipoplexes membrane ruffling and actin reorganization assay was performed. Fig. 5 (control) represents highly organized actin filaments at the periphery and in the cytoskeleton of untreated breast cancer cells. When the anionic lipoplexes (AF1 or AF2) were added, ribbon like structures and membrane protrusions accompanied by actin rearrangement within the cytoskeleton, were evident (Fig. 5). In the case of CF, actin reorganization was observed but membrane ruffles were absent. Since all the lipoplexes (anionic and cationic) induced actin rearrangement, their uptake was actin-mediated.

Uptake of the anionic lipoplexes was examined in the presence of cytochalasin D that prevents actin polymerization (23). As shown in Fig. 3d, e, incubation of cytochalasin D treated cells with anionic lipoplexes reduced the uptake of AF2 by 87% whereas AF1 uptake was unaffected. Uptake of CF was inhibited by 64% with cytochalasin D (Fig. 3f). These observations were in consensus with the fluorescence microscopy results shown in Fig. 4. With respect to the anionic liposome control, its uptake was reduced by 95% in the presence of cytochalasin D (Supplementary Material Fig. S4). However, the uptake of the Ca^{2+}-siRNA control was unaffected (Supplementary Material Fig. S4) as was the case for AF1.

In case of the AF1 formulation, the results obtained from the membrane ruffling assay and the cytochalasin D inhibition assay were paradoxical. To investigate this further, the effect of AF1 on actin polymerization was evaluated in the

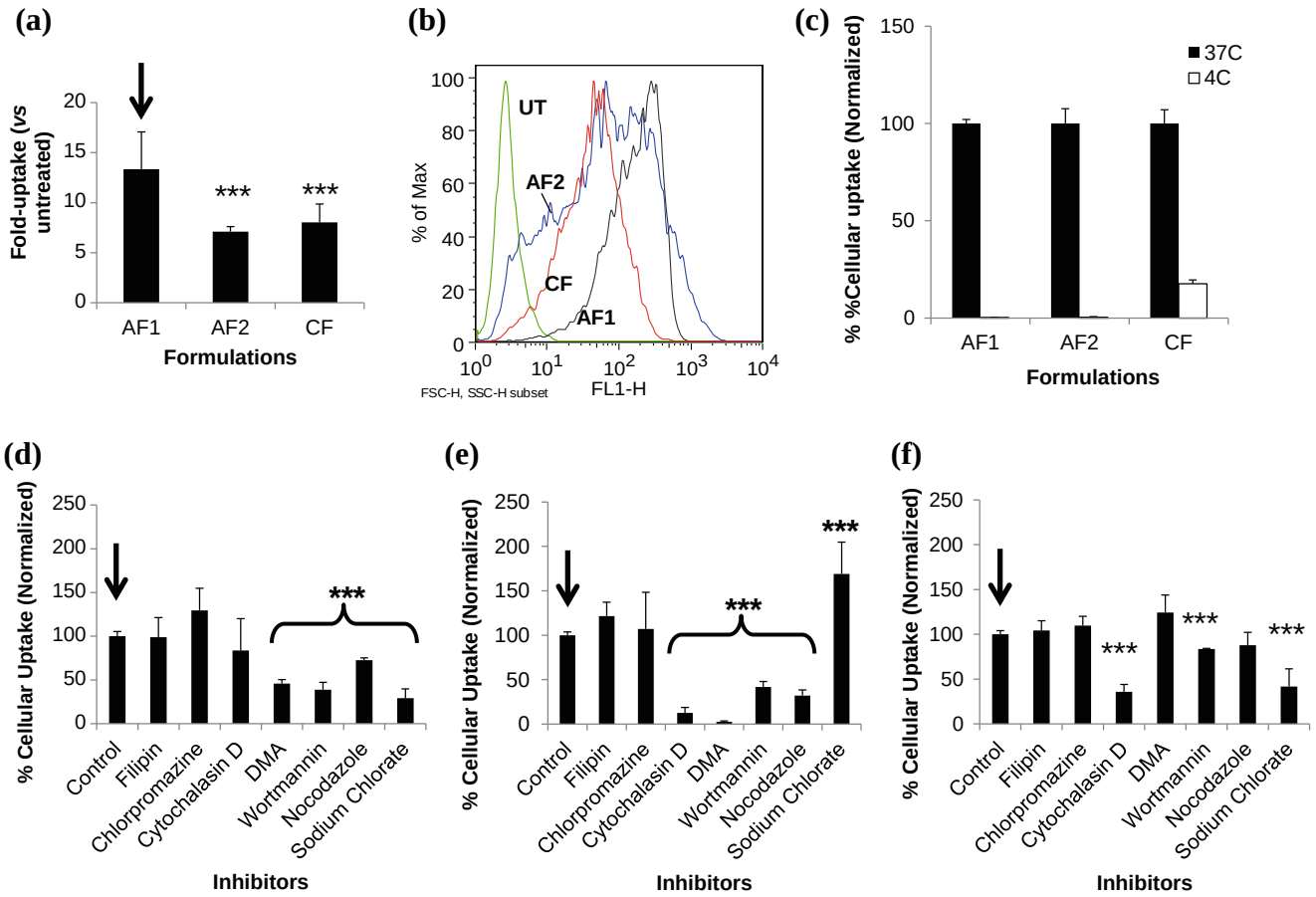

Fig. 3 FACS analysis indicating cellular uptake of the lipoplexes (AF1, AF2, CF) in breast cancer cells. (**a**) Fold-uptake of lipoplexes normalized to untreated cells. (**b**) Histograms representing relative uptake of AF1 (*black line*), AF2 (*blue line*), CF (*red line*). Untreated cells were used as a negative control (*green line*). (**c**) Percentage cellular uptake of lipoplexes at 37°C or 4°C. Percentage cellular uptake of: (**d**) AF1; (**e**) AF2; and (**f**) CF, in the presence or absence of various pharmacological inhibitors. Cells were pre-incubated with inhibitors for 30 min (sodium chlorate for 24 h) followed by incubation with lipoplexes (40 nM alexa-488 siRNA) for 4 h. Control samples represent the cells transfected with lipoplex formulations in the absence of inhibitors. Percentage cellular uptake was obtained after normalizing the cells to the fluorescence uptake of the controls (considered as 100%). ***$p < 0.001$. Arrows indicate the control groups used for comparison. The results are the average of three independent experiments each time in duplicate. Mean ± SD.

presence of cytochalasin D. As shown in Fig. 6, in the absence of cytochalasin D (control), organized actin filaments were clearly observed. On the addition of cytochalasin D, depolymerization of actin was evident from the absence of actin fibers at the periphery and in the cytoskeleton. Instead, actin monomers and oligomers were observed bundled together at the edges (Fig. 6, 0 h). Actin in the cells remained depolymerized even after 4 h, in the presence of the drug (Fig. 6, 4 h). When the actin depolymerized cells were incubated with AF1 for 4 h, polymerization of actin (in a reorganized fashion) was evident (Fig. 6, AF1). Similar observations were made with the Ca^{2+}-siRNA control and the calcium alone. However, for AF2, CF or the anionic liposome (an-lip) control, this was not evident.

The role of the microtubules in the internalization of the anionic lipoplexes was investigated using nocodazole (causes microtubule disruption) (24). Fluorescence microscopy showed considerable reduction in the uptake of both AF1 and AF2 lipoplexes with nocodazole (Fig. 4). FACS analysis showed uptake inhibition to be 27% and 68% for AF1 and AF2, respectively (Fig. 3d, e). On the contrary, uptake of CF was unaffected by nocodazole (Fig. 3f and 4). Therefore, microtubules participate in the uptake of the anionic lipoplexes (AF1, AF2) but not the cationic lipoplexes (CF).

On evaluating the uptake of the anionic lipoplexes in the presence of sodium chlorate (HSPG inhibitor), FACS analysis showed a 71% reduction in the uptake of AF1 (Fig. 3d). In contrast, the uptake of AF2 was not inhibited (Fig. 3e). Instead, there was a significant increase in the uptake of these formulations with sodium chlorate. Such an increase was also observed with the anionic liposome control (Supplementary Material Fig. S4). As in the case of AF1, the uptake of CF was also inhibited (by 58%) (Fig. 3f). These results were in consensus with the microscopic observations that showed significant reduction in the

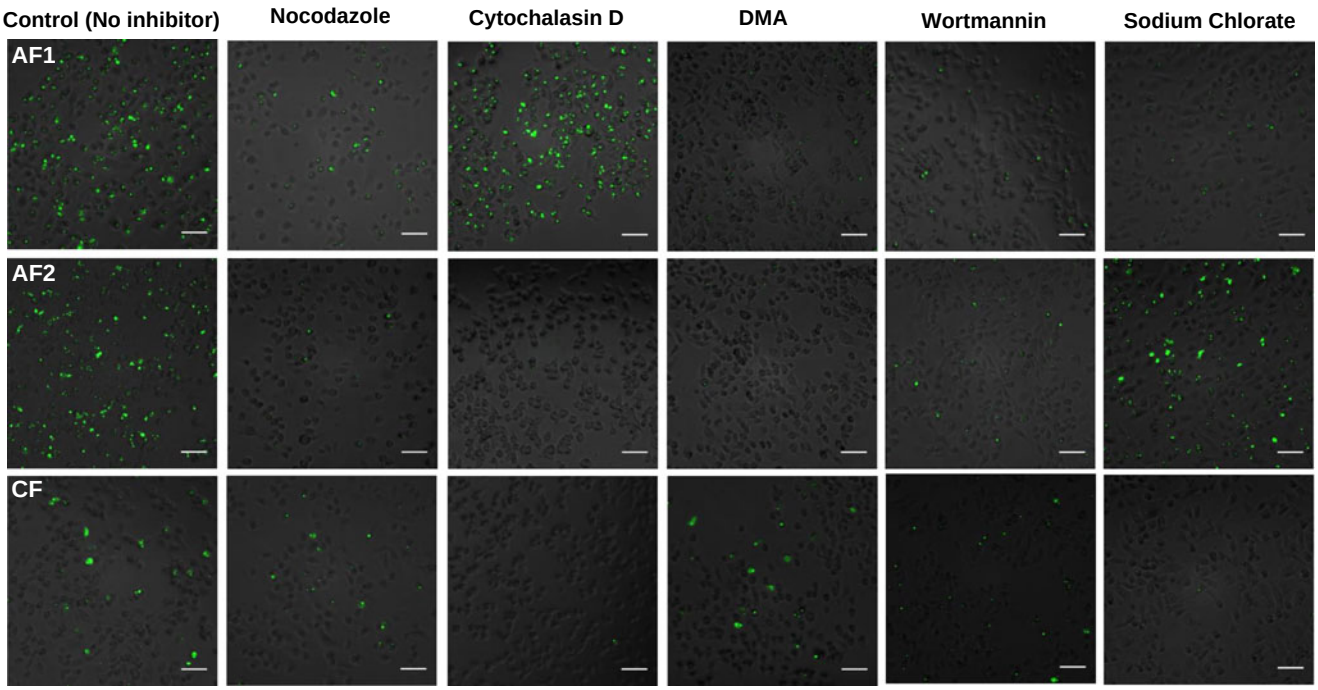

Fig. 4 Fluorescence microscopy images representing cellular uptake of lipoplex formulations (AF1, AF2, CF) in the presence or absence of various inhibitors incubated with cells for 30 min (sodium chlorate 24 h), followed by lipoplex incubation for 4 h. Control samples represent the cells transfected with formulations in the absence of inhibitors. One image (out of five) was selected to represent the sample. Camera settings and image adjustments were kept constant for control and treated samples to achieve an accurate comparison. AF1 and CF were prepared with 14 nM alexa 488-siRNA and AF2 was prepared with 56 nM alexa 488-siRNA. Scale bar 100 μm.

uptake of AF1 and CF with sodium chlorate (Fig. 4). As with AF1, the uptake of the Ca^{2+}-siRNA control was also reduced with sodium chlorate (Supplementary Material Fig. S4).

It is important to note that during the inhibition studies, blocking one particular pathway at a time did not cause 100% inhibition with any formulation (except

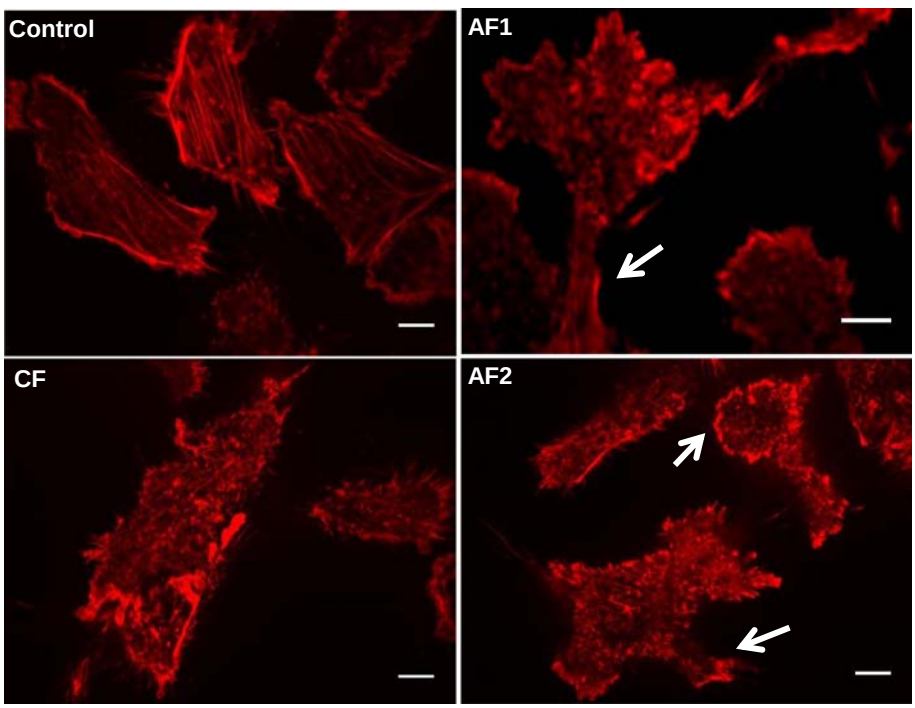

Fig. 5 Confocal images of serum starved breast cancer cells (ventral region) incubated with lipoplexes (AF1, AF2, CF) for 30 min followed by fixation and actin labeling with alexa-647 phalloidin (red). Control sample represents highly organized actin fibers in cells in the absence of lipoplexes. White arrows indicate membrane ruffles and protrusions induced by AF1 and AF2. Actin rearrangement was observed with CF. Scale bar: 10 μm.

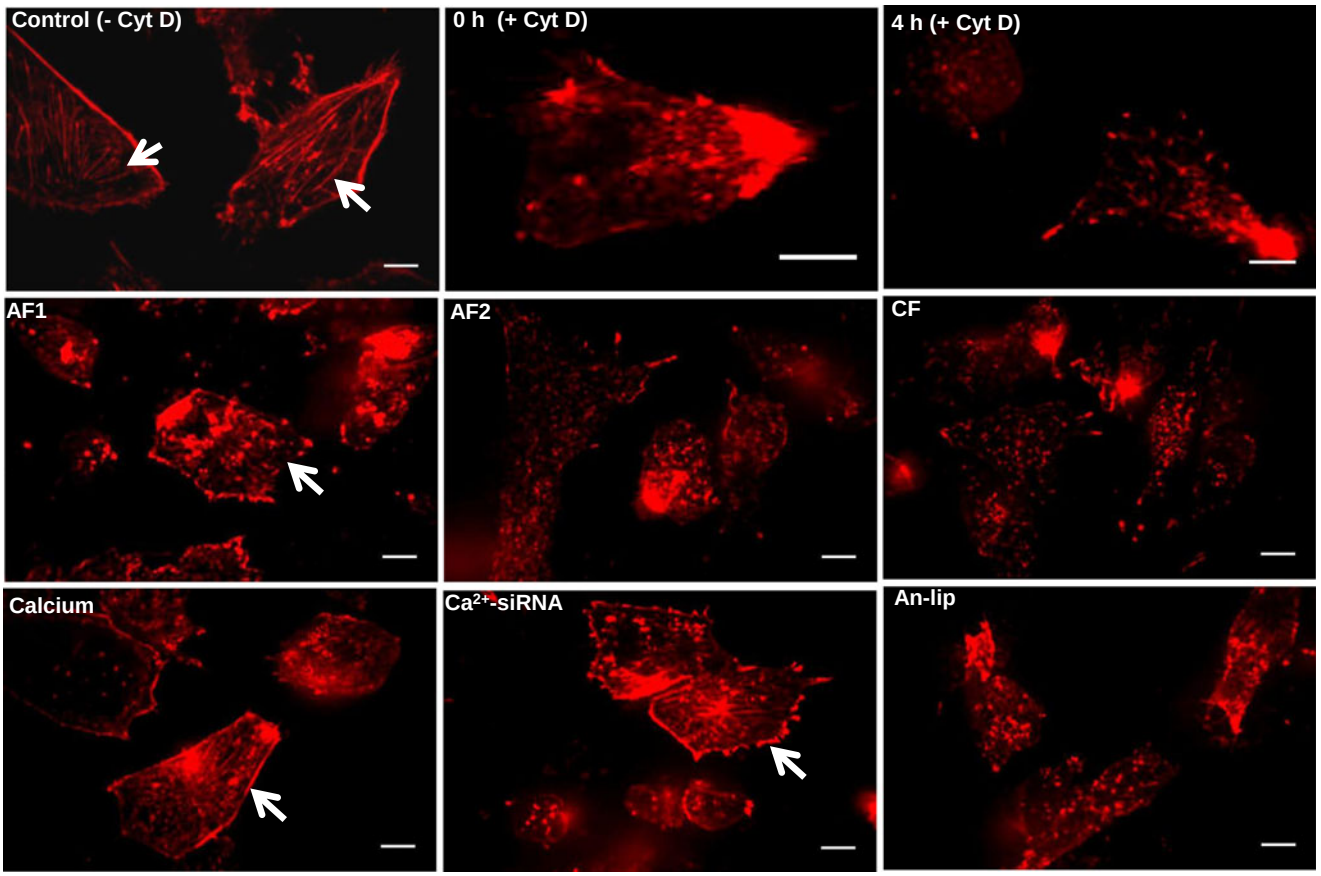

Fig. 6 Confocal images indicating the effect of various lipoplex formulations (AF1, AF2, CF) on polymerization of actin in the presence of cytochalasin D (prevents actin polymerization). The cells were incubated with cytochalasin D (Cyt D) for 30 min followed by incubation with lipoplexes (40 nM siRNA) for 4 h. After washing and trypan blue quenching, the cells were fixed, made more permeable with 0.3% TX100, and labeled with alexa-647 phalloidin (*red*). The control represent the cells not treated with cytochalasin D or lipoplexes. 0 h and 4 h samples are the cells treated with cytochalasin D but not with lipoplexes, visualized immediately and after 4 h, respectively. Phalloidin stained actin was also observed for the cells incubated for 4 h with calcium alone, Ca^{2+}-siRNA control (Ca^{2+}/siRNA ratio of 2.5/1) or anionic liposome control (an-lip). White arrows indicate the actin fibers. Scale bar: 10 μm

with AF2) suggesting simultaneous participation of multiple pathways in the uptake process.

Co-localization Studies

Co-localization of alexa-488 siRNA in lipoplexes, was observed with the endocytic markers. Since macropinocytosis was involved in the uptake process, dextran was used as the marker for the macropinosomes and this was confirmed when its uptake was 95–100% inhibited in the presence of cytochalasin D, DMA or wortmannin (data not shown). Also CTB, a known marker for caveolae-mediated uptake (abundant in lipid rafts) was used as a control (20). For this purpose, the cells were incubated with the lipoplexes (AF1, AF2 or CF) and the endocytic marker simultaneously and visualized using confocal microscopy. Fig. 7a represents formulation co-localization with dextran in the cell interior (central z-section) and the entire cell (maximum intensity z-projection or MIP). Both the central z-section and the MIP images indicated significant co-localization (yellow/white region) of dextran with AF1 and AF2 indicating that macropinocytosis is involved in uptake of these lipoplexes (Fig. 7a). These results are in consensus with the results from the inhibition studies (Fig. 3d, e). It can also be observed that the extent of co-localization of dextran with AF2 was significantly greater than with AF1 (comparing the white regions). To confirm this, the images were quantified and the data was represented in terms of correlation coefficients (MCC, PCC). Accordingly, the MCC and PCC values for AF1 were 0.4 and 0.3, respectively. In the case of AF2, the MCC value was 0.8 whereas the PCC value was 0.4 (Fig. 7b). Higher correlation values for AF2 compared to AF1 indicated a greater degree of co-localization of dextran with AF2. This suggests a larger contribution of macropinocytosis towards the uptake of AF2 compared to AF1. Again, this conclusion is in agreement with the inhibition studies that showed greater uptake inhibition of AF2 with DMA, when compared to AF1 (Fig. 3d, e). In the case of CF, co-localization with dextran was sparse as indicated by coefficient values of less than 0.2 (Fig. 7b).

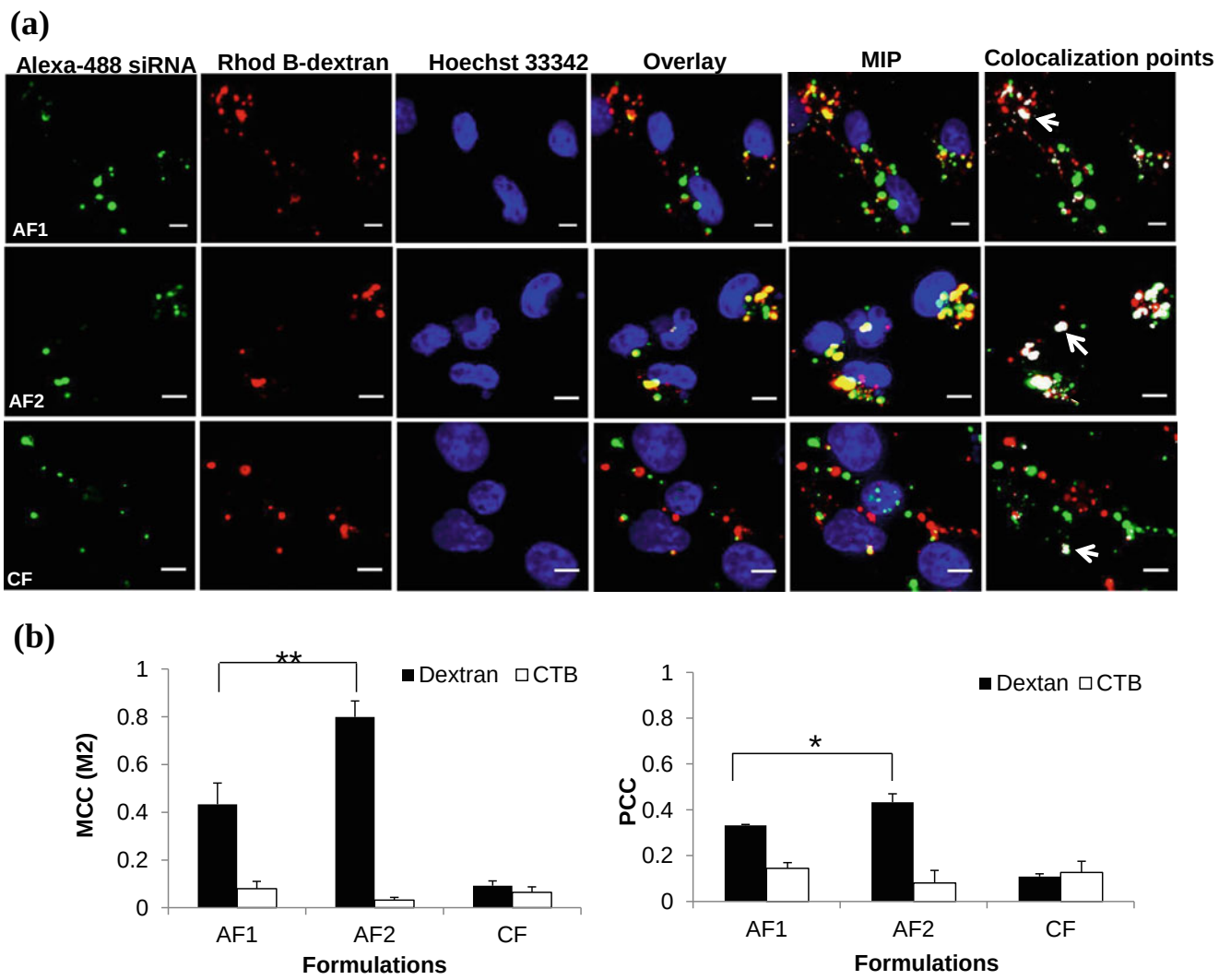

Fig. 7 (**a**) Confocal images representing co-localization of lipoplex formulations (AF1, AF2, CF) with the macropinocytosis marker, dextran. The cells were incubated with green alexa-488 siRNA lipoplexes (40 nM siRNA) for 2 h and dextran (*red*) was added in the last 0.5 h. The cells were washed with HBSS, quenched with trypan blue and the nucleus was stained (*blue*) before live cell imaging. The presented data is the central z-section of the cells, shown in separate channels as well as the overlay image. Maximum intensity z-projection (MIP) represents co-localization of lipoplexes with dextran in the entire cell. Co-localization points were obtained from MIP image using the Image J software. Scale bar: 10 μm. (**b**) Quantification of the extent of co-localization of lipoplexes with dextran (macropinocytosis marker) using Pearson's correlation coefficient (PCC) and Mander's correlation coefficient (MCC) that was calculated using the JACoP plugin in the Image J software. M2 (in MCC) is the extent of red overlap with green. The results were an average of quantification from 5 fields of view/samples with 2–6 cells/view. $^{**}p < 0.01$, $^{*}p < 0.05$. Mean ± SD.

With respect to co-localization with the caveolae marker (CTB), all formulations showed negligible co-localization as indicated by the confocal images and the quantification data (Supplementary Material Fig. S5). These results are in consensus with the inhibition studies that showed uptake of the lipoplex formulations to be unaffected by filipin (Fig. 3).

It should be noted that the co-localization correlation coefficient, MCC is based on signal co-existence (independent of relative signal intensities) whereas PCC is based on signal proportionality (dependent on relative signal intensities) (18). In this work, there was a significant difference between the intensities of the green (siRNA) and the red (markers) signals and therefore MCC was considered as a more accurate measurement. True representation of MCC was verified by its ability to correlate with the confocal data (Fig. 7 and Supplementary Material Fig. S5), as opposed to PCC.

Silencing efficiency and P/D ratios of the lipoplex formulations revealed that silencing efficiency of AF1 formulation was significantly greater than the AF2 formulation (Table III). On the contrary, P/D ratio of AF1 was significantly lower than the AF2 formulation indicating the greater endosomal escaping capability of the former (the P/D ratio is inversely proportional to the endosomal escaping capability). The silencing efficiency of the CF formulation was comparable to the AF1 formulation. However, the CF formulation showed highest endosomal escaping efficiency

Table III Endosomal Escaping Capability (P/D ratio) and Silencing Efficiency of Various Lipoplex Formulations

Formulations	Ca2+/siRNA ratio	P/D ratio [a]	Silencing Efficiency (%) [b]
AF2	0.3/1	2.32	10.2 ± 5.6
AF1	2.5/1	0.18	71.7 ± 3.9
CF	-	0.02	55.79 ± 13.71

[a] P/D ratio was calculated by quantifying confocal images obtained with a 40X objective using the Image J software. Each ratio is an average from 5 fields of view per sample. The detailed quantification method has been published previously (9)

[b] The silencing efficiency was evaluated using the previously published method (9)

of the three formulations (lowest P/D ratio). Negative controls showed negligible silencing efficiency (data not shown).

It should be noted that only for silencing efficiency studies, anti-eGFP siRNA was used whereas for all the other studies alexa-488 siRNA was used. Although the sequence of these two siRNAs is different, their cellular interaction (intra- and extra) would be similar due to the following reasons: a) Both siRNAs have the same nucleotide length (21 bases with 2NT 3′ overhangs) and, b) both siRNAs have similar GC content (between 40 and 60%). Accordingly, we do not anticipate any significant difference between their interaction with Ca^{2+} and anionic lipids during lipoplex formation. This is supported by the fact that lipoplexes prepared with either siRNA showed similar physicochemical characteristics – particle size and surface charge (data not shown). Therefore, silencing efficiency results with anti-eGFP siRNA can be related to the uptake mechanism and endosomal release results obtained with alexa-488 siRNA.

DISCUSSION

The internalization mechanism of novel anionic lipoplex formulations (anionic liposomes, calcium and siRNA) was elucidated using both inhibition and co-localization approaches. AF1 and AF2 formulations differed in calcium levels with higher calcium in the former.

The low temperature inhibition studies were able to decipher non-endocytic uptake of the lipoplex formulations since endocytosis (an energy and temperature dependent process) does not occur at low temperature (13), whereas membrane fusion (that involves lipid mixing) may occur at low temperatures (25). Accordingly, since uptake of the anionic lipoplexes (AF1 and AF2) was completely inhibited at 4°C this suggests that these lipoplexes are only taken up by endocytic pathways (Fig. 3c). On the other hand, some portion of cationic lipoplexes (CF) must enter *via* membrane fusion since CF uptake inhibition at low temperature was only 83%. This is in agreement with several reports that have shown uptake of different cationic lipoplexes *via* membrane fusion (12,26).

Uptake of all the lipoplexes (AF1, AF2, CF) appeared to be clathrin and caveolae-independent due to their observed insensitivity to chlorpromazine and filipin treatment as well as their poor co-localization with the caveolae marker (CTB) (Supplementary Material Fig. S5). Accordingly, involvement of a clathrin and caveolae-independent pathway, (heparin sulfate proteoglycans or HSPG) was examined using sodium chlorate (27,28). The uptake of CF was inhibited by sodium chlorate indicating that the HSPG-mediated pathway is involved in the uptake of these cationic lipoplexes. HSPGs have been shown to interact with cationic nanoparticles *via* electrostatic interactions, facilitating cellular uptake (16). As in the case of CF AF1 was also taken up *via* the HSPG pathway as indicated by significant uptake inhibition (~70%) in the presence of sodium chlorate (Fig. 3d). This was probably due to electrostatic interaction between anionic HSPGs and the excess calcium in the AF1 formulation (anionic lipid/Ca^{2+}/siRNA ratio of 1.3/2.5/1). This hypothesis is supported by the fact that the Ca^{2+}-siRNA control (Ca^{2+}/siRNA ratio of 2.5/1) was also taken up *via* the HSPG pathway due to its sensitivity to sodium chlorate (Supplementary Material Fig. S4). The excess calcium in AF1 appears to participate in the uptake process despite a negative zeta potential (Table II) indicating that calcium is not covering the entire lipoplex surface. However, the amount of calcium appears to be sufficient to allow interaction with HSPGs on the cell surface. It can therefore be concluded that surface charge does not necessarily determine the uptake pathway.

On the contrary, the uptake of AF2 (lower calcium levels) and of the anionic liposome control was not inhibited with sodium chlorate. Instead, their uptake (Fig. 3e, Supplementary Material Figs. S3 and S4) increased in the presence of sodium chlorate. This is probably due to the absence of anionic heparin sulfate groups which are responsible for electrostatic repulsion allowing non-specific uptake of the anionic nanoparticles (AF2, anionic liposomes). The 30% uptake of AF1 in the presence of sodium chlorate is probably due to non-specific uptake as a result of lack of repulsion with the cell surface as well as uptake *via* other pathways.

Irrespective of their composition, anionic lipoplexes (AF1 and AF2) were taken up *via* macropinocytosis as indicated by their significant uptake inhibition with DMA and wortmannin (Fig. 3d, e). This was supported by significant co-localization of these lipoplexes with the macropinosome marker, dextran (Fig. 7). Additionally, membrane ruffles with peripheral protrusions (characteristic features of macropinocytosis (22,29)), were evident in the cells incubated with anionic lipoplexes (Fig. 5). Furthermore, the uptake of the anionic lipoplexes was mediated by microtubules

(uptake inhibition with nocodazole) (Fig. 3d, e and Supplementary Material Fig. S3) that are known to participate in macropinocytosis (30). Despite a significant difference in the particle size of AF1 and AF2 (Table II), their uptake occurred *via* macropinocytosis as this pathway is known to take up particles from the nanometer to the micron range (22). Uptake of CF, on the other hand, was not macropinocytic as evident from its insensitivity to DMA (Fig. 3f and Supplementary Material Fig. S3), a selective macropinocytosis inhibitor, as well as the absence of membrane ruffles (Fig. 5). However, uptake of CF was actin-dependent as indicated by actin rearrangement (Fig. 5) and uptake inhibition with cytochalasin D (Fig. 3f). This actin-dependent process could be phagocytic as evident from the phase contrast images that showed phagocytic cup-like vesicles (31) in those cells incubated with CF (Fig. 2b). The morphology of these vesicles was distinct from the vesicles (macropinosomes) formed with AF2 as indicated by comparatively prominent pits in the former due to the double wall (32). The phagocytic cups were perinuclear and not peripheral as these images were obtained 4 h post-incubation (Fig. 2b). Again, ligand-receptor interaction, a critical parameter for phagocytosis (33). was apparent from the fact that CF uptake was inhibited by wortmannin, an inhibitor of PI3K that participates in FcγR receptor-mediated phagocytosis (33). It was also interesting to note that only 16% uptake occurred *via* FcγR receptor-mediated phagocytosis (Fig. 3f) suggesting the possible involvement of other receptor-mediated uptake processes. Interestingly, the phagocytic uptake of CF was observed to be microtubule-independent (Fig. 3f and Supplementary Material Fig. S3). Microtubules are required for certain types of phagocytosis, but not all. For example Schagat *et al.* have shown that phagocytosis by alveolar macrophages is microtubule-independent (34). The specificity of the phagocytic process was evident from the fact that it was responsible for uptake of only one (CF) of the three formulations (AF1, AF2, CF). Cellular uptake of the cationic lipoplexes (CF) *via* phagocytosis and of the anionic lipoplexes *via* macropinocytosis suggests the influence of the delivery carrier on the uptake pathway.

Macropinocytosis being non-receptor mediated is generally considered as a non-specific uptake pathway (22). Despite being non-specific, macropinocytosis has been shown to be the dominant uptake pathway for certain nanomaterials. For example, anionic and neutral liposomes have been shown to be taken up more efficiently *via* macropinocytosis when compared to cationic liposomes (35). This may explain why the anionic lipoplexes (AF2) and the anionic liposome (control) were taken up *via* macropinocytosis in contrast to the cationic ones (CF) (Fig. 3 and 7). Interestingly, the uptake of AF1 formulation was also macropinocytic probably due to the involvement of excess calcium in this uptake process. This assumption is corroborated by the fact that uptake of the Ca^{2+}-siRNA control was also reduced in the presence of DMA (macropinocytosis inhibitor) (Supplementary Material Fig. S4). In agreement with these results, calcium phosphate nanoparticles have been shown to be taken up by macropinocytosis (36). It was also interesting to note that the contribution of macropinocytosis towards the uptake of the anionic lipoplexes decreased with an increase in the Ca^{2+}/siRNA ratio. For example, DMA inhibition studies indicated nearly 98% uptake of AF2 but only 54% uptake of AF1 *via* macropinocytosis. This is probably due to the interaction of excess calcium (in AF1) with HSPG resulting in partial uptake *via* the HSPG pathway. This outcome shows that minor changes in formulation may affect the cellular uptake mechanism. It is also clear that surface charge does not necessarily determine the uptake mechanism.

Uptake of all three lipoplexes (AF1, AF2, CF) was actin-dependent as evidenced by the presence of reorganized actin filaments and/or membrane ruffles (Fig. 5). Despite this fact, the uptake of AF1 was unaffected by the actin depolymerizer, cytochalasin D (Fig. 3d). Additionally, phase contrast microscopy showed cytochalasin D-treated cells to be less round when incubated with AF1 when compared to AF2 (Fig. 4), suggesting that AF1 may be counteracting the effect of cytochalasin D. Prominent actin fibers (in a reorganized manner suggesting actin-mediated uptake) were observed in cells incubated with cytochalasin D and AF1 but not in cells incubated with cytochalasin D and AF2. Since AF1 and AF2 differ only in the calcium concentration, it is speculated that the excess calcium plays a role in fiber formation *via* actin polymerization. Similar actin filaments (polymers) were observed with the Ca^{2+}-siRNA control and an additional control where only calcium was added (Fig. 6). This polymerization was due to the calcium and not due to the positive charge as indicated by the absence of such actin fibers in the presence of cationic lipoplexes (CF) (Fig. 6). Accordingly, it was concluded that the excess calcium in AF1 contributed to the actin polymerization against the effect of cytochalasin D. These results are in agreement with the work of Tellam *et al.* that showed induction of actin polymerization due to calcium chloride (37).

The present studies have revealed the uptake of lipoplexes by various pathways based on their formulation compositions. The AF2 formulation (low calcium levels) was taken up by macropinocytosis, whereas the uptake of the AF1 formulation (high calcium levels) was *via* macropinocytosis as well as the HSPG pathway. The CF formulation was taken up by phagocytosis, the HSPG pathway and by membrane fusion. These findings are helpful in identifying the rate-limiting steps to efficient intracellular delivery and consequently in improving delivery efficiency. For example, except membrane fusion, all the aforementioned pathways involve endo/lysososomal compartments (16,22,38). Therefore, efficient endosomal escape is

required (rate-limiting) to obtain effective cytoplasmic delivery of siRNA when internalized by these pathways. It was evident from the punctate to diffused staining (P/D) ratios (Table III) of the three lipoplex formulations, that the efficiency of endosomal release of the CF formulation was maximum (lowest P/D ratio) whereas the AF2 formulation (highest P/D ratio) was minimum. This indicates that the AF2 formulation has poor endosomal escape and it can be speculated that this along with low siRNA loading efficiency (Table II) is the cause of the negligible silencing (Table III) of this formulation despite its high cellular uptake (Fig. 3a). The AF1 formulation showed high silencing due to better endosomal release and higher siRNA loading compared to AF2 (lower P/D ratio, Table III). It is speculated that the higher calcium levels of the AF1 formulation may be responsible for the improved endosomal release. A previous publication has shown that calcium facilitates endosomal escape of nucleic acids (39). Although the silencing efficiencies of the AF1 and CF formulations were comparable, (Table III) it is apparent from the trafficking studies that this was achieved by different pathways. In the case of the CF formulation fewer cells participated in the uptake process (Fig. 4) and the percentage uptake was consequently less compared to the AF1 formulation (Fig. 3a). However, the CF formulation was more efficient in delivering the siRNA to the cytoplasm as evident from its low P/D ratio (Table III). This is due at least in part to the portion of the CF formulation that was taken up by membrane fusion (direct cytoplasmic entry) (Fig. 3c). In addition, the portion of CF formulation that is taken up by the phagocytosis and HSPG pathways may have better endo/lysosomal escape compared to the AF1 formulation. The AF1 formulation showed high cellular uptake but less efficient endosomal escape compared to the CF formulation. This information may be utilized to improve the silencing efficiency of siRNA delivery systems. For example, the AF1 formulation could be modified to enhance the endosomal escape such as by incorporating a higher proportion of DOPE (fusogenic lipid) in the formulation. Alternatively, the AF1 formulation could be modified for targeted delivery *via* a non-acidic pathway such as caveolae. For this purpose, certain moieties known to be taken up by the caveolae-pathway such as folic acid could be incorporated into the formulation (40). Yet another approach to achieve enhanced silencing efficiency could be formulation modification to achieve delivery *via* a non-endocytic pathway such as membrane fusion.

CONCLUSIONS

Cellular uptake pathways of novel anionic lipoplexes were investigated as a function of formulation composition. Changes in composition influenced the formulation-cell interaction thereby affecting the cellular uptake mechanism. Elucidation of uptake mechanism studies helped in understanding the role of formulation components on uptake and consequent bioactivity. These studies revealed that some of the uptake processes such as phagocytosis, membrane fusion and microtubular transport were delivery vector dependent, whereas others such as the HSPG pathway were delivery vector independent for those vectors investigated. To the best of our knowledge, this is the first time that cellular uptake pathways of lipoplexes prepared with anionic liposomes (along with calcium) as well as with the commonly used Lipofectamine^{TM}2000 transfection reagent have been investigated. Understanding of the internalization mechanism and activity of the formulations facilitated identification of roadblocks to efficient intracellular siRNA delivery. Such mechanistic studies are essential for the rational development of carriers to accomplish enhanced nucleic acid delivery.

ACKNOWLEDGMENTS AND DISCLOSURES

The authors would like to thank Dr. Carol Norris, Biotechnology Bioservices Center, University of Connecticut, Storrs, CT, for assistance with FACS and confocal microscopy experiments; Dr. Renee Gilberti for useful scientific discussions and Alnylam Pharmaceuticals, Cambridge, MA for the gift of alexa-488 siRNA.

REFERENCES

1. Kumar P, Ban HS, Kim SS, Wu H, Pearson T, Greiner DL, *et al.* T cell-specific siRNA delivery suppresses HIV-1 infection in humanized mice. Cell. 2008;134(4):577–86.
2. Oh YK, Park TG. siRNA delivery systems for cancer treatment. Adv Drug Deliv Rev. 2009;61(10):850–62.
3. Wang J, Lu Z, Wientjes M, Au J. Delivery of siRNA Therapeutics: Barriers and Carriers. AAPS J. 2010;12(4):492–503.
4. Kapoor M, Burgess DJ, Patil SD. Physicochemical characterization techniques for lipid based delivery systems for siRNA. Int J Pharm. 2012;427(1):35–57.
5. Wasungu L, Hoekstra D. Cationic lipids, lipoplexes and intracellular delivery of genes. J Control Release. 2006;116(2):255–64.
6. Kedmi R, Ben-Arie N, Peer D. The systemic toxicity of positively charged lipid nanoparticles and the role of Toll-like receptor 4 in immune activation. Biomaterials. 2010;31(26):6867–75.
7. Patil SD, Rhodes DG, Burgess DJ. Anionic liposomal delivery system for DNA transfection. AAPS J. 2004;6(4):e29.
8. Srinivasan C, Burgess DJ. Optimization and characterization of anionic lipoplexes for gene delivery. J Control Release. 2009;136 (1):62–70.
9. Kapoor M, Burgess DJ. Efficient and safe delivery of siRNA using anionic lipids: formulation optimization studies. Int J Pharm. 2012;432(1–2):80–90.
10. Kapoor M, Burgess DJ. Physicochemical characterization of anionic lipid-based ternary siRNA complexes. Biochim et Biophys Acta (BBA) - Biomembr. 2012;1818(7):1603–12.

11. Khalil IA, Kogure K, Akita H, Harashima H. Uptake Pathways and Subsequent Intracellular Trafficking in Nonviral Gene Delivery. Pharmacol Rev. 2006;58(1):32–45.
12. Lu JJ, Langer R, Chen J. A novel mechanism is involved in cationic lipid-mediated functional siRNA delivery. Mol Pharm. 2009;6 (3):763–71.
13. Bentz J. Intermediates and kinetics of membrane fusion. Biophys J. 1992;63(2):448–59.
14. Punnonen EL, Ryhanen K, Marjomaki VS. At reduced temperature, endocytic membrane traffic is blocked in multivesicular carrier endosomes in rat cardiac myocytes. Eur J Cell Biol. 1998;75(4):344–52.
15. Sahay G, Alakhova DY, Kabanov AV. Endocytosis of nanomedicines. J Control Release. 2010;145(3):182–95.
16. Payne CK, Jones SA, Chen C, Zhuang X. Internalization and trafficking of cell surface proteoglycans and proteoglycan-binding ligands. Traffic. 2007;8(4):389–401.
17. Rejman J, Bragonzi A, Conese M. Role of Clathrin- and Caveolae-Mediated Endocytosis in Gene Transfer Mediated by Lipo- and Polyplexes. Mol Ther. 2005;12(3):468–74.
18. Bolte S, Cordelieres FP. A guided tour into subcellular colocalization analysis in light microscopy. J Microsc. 2006;224(Pt 3):213–32.
19. Abbineni G, Modali S, Safiejko-Mroczka B, Petrenko VA, Mao C. Evolutionary selection of new breast cancer cell-targeting peptides and phages with the cell-targeting peptides fully displayed on the major coat and their effects on actin dynamics during cell internalization. Mol Pharm. 2010;7(5):1620–42.
20. Orlandi PA, Fishman PH. Filipin-dependent inhibition of cholera toxin: evidence for toxin internalization and activation through caveolae-like domains. J Cell Biol. 1998;141(4):905–15.
21. Koivusalo M, Welch C, Hayashi H, Scott CC, Kim M, Alexander T, *et al.* Amiloride inhibits macropinocytosis by lowering submembranous pH and preventing Rac1 and Cdc42 signaling. J Cell Biol. 2010;188(4):547–63.
22. Maniak M. Macropinocytosis. In: Marsh M, editor. Endocytosis, vol. 1. Great Britain: Oxford University Press; 2001. p. 78–87.
23. Casella JF, Flanagan MD, Lin S. Cytochalasin D inhibits actin polymerization and induces depolymerization of actin filaments formed during platelet shape change. Nature. 1981;293 (5830):302–5.
24. Zieve GW, Turnbull D, Mullins JM, McIntosh JR. Production of large numbers of mitotic mammalian cells by use of the reversible microtubule inhibitor Nocodazole: Nocodazole accumulated mitotic cells. Exp Cell Res. 1980;126(2):397–405.
25. Chernomordik LV, Zimmerberg J. Bending membranes to the task: structural intermediates in bilayer fusion. Curr Opin Struct Biol. 1995;5(4):541–7.
26. Noguchi A, Furuno T, Kawaura C, Nakanishi M. Membrane fusion plays an important role in gene transfection mediated by cationic liposomes. FEBS Lett. 1998;433(1–2):169–73.
27. Delehedde M, Deudon E, Boilly B, Hondermarck H. Heparan sulfate proteoglycans play a dual role in regulating fibroblast growth factor-2 mitogenic activity in human breast cancer cells. Exp Cell Res. 1996;229(2):398–406.
28. Garud DR, Tran VM, Victor XV, Koketsu M, Kuberan B. Inhibition of heparan sulfate and chondroitin sulfate proteoglycan biosynthesis. J Biol Chem. 2008;283(43):28881–7.
29. Nakase I, Niwa M, Takeuchi T, Sonomura K, Kawabata N, Koike Y, *et al.* Cellular uptake of arginine-rich peptides: roles for macropinocytosis and actin rearrangement. Mol Ther. 2004;10(6):1011–22.
30. Waterman-Storer CM, Worthylake RA, Liu BP, Burridge K, Salmon ED. Microtubule growth activates Rac1 to promote lamellipodial protrusion in fibroblasts. Nat Cell Biol. 1999;1(1):45–50.
31. Swanson JA, Johnson MT, Beningo K, Post P, Mooseker M, Araki N. A contractile activity that closes phagosomes in macrophages. J Cell Sci. 1999;112(Pt 3):307–16.
32. Swanson JA. Shaping cups into phagosomes and macropinosomes. Nat Rev Mol Cell Biol. 2008;9(8):639–49.
33. Caron E, Hall A. Phagocytosis. In: Marsh M, editor. Endocytosis, vol. 1. Great Britain: Oxford University Press; 2001. p. 58–71.
34. Schagat TL, Tino MJ, Wright JR. Regulation of protein phosphorylation and pathogen phagocytosis by surfactant protein A. Infect Immun. 1999;67(9):4693–9.
35. Isenberg G. Actin binding proteins–lipid interactions. J Muscle Res Cell Motil. 1991;12(2):136–44.
36. Schmidt SM, Moran KA, Tweed Kent AM, Slosar JL, Webber MJ, McCready MJ, *et al.* Uptake of calcium phosphate nanoshells by osteoblasts and their effect on growth and differentiation. Journal of Biomedical Materials Research Part A. 2008;87A:418–28.
37. Tellam R. Mechanism of CaCl2-induced actin polymerization. Biochemistry. 1985;24(16):4455–60.
38. Wadia JS, Stan RV, Dowdy SF. Transducible TAT-HA fusogenic peptide enhances escape of TAT-fusion proteins after lipid raft macropinocytosis. Nat Med. 2004;10(3):310–5.
39. Kulkarni VI, Shenoy VS, Dodiya SS, Rajyaguru TH, Murthy RR. Role of calcium in gene delivery. Expert Opin Drug Deliv. 2006;3 (2):235–45.
40. Sabharanjak S, Mayor S. Folate receptor endocytosis and trafficking. Adv Drug Deliv Rev. 2004;56(8):1099–109.